Topological transition and edge states in HgTe quantum wells from first principles

Sebastian Küfner* and Friedhelm Bechstedt
Institut für Festkörpertheorie und -optik, Friedrich-Schiller-Universität,
and European Theoretical Spectroscopy Facility (ETSF), Max-Wien-Platz 1, 07743 Jena, Germany
(Received 26 March 2014; published 28 May 2014)

$(HgTe)_N(CdTe)_M(110)$ and (001) superlattices are studied by means of *ab initio* calculations versus the thickness of the HgTe quantum wells (QWs). The used approximate quasiparticle theory including spin-orbit coupling (SOC) gives the correct band ordering, band gap, and SOC splitting for bulk HgTe and CdTe. The resulting band discontinuities indicate confinement also for occupied states. In agreement with earlier $\mathbf{k}\cdot\mathbf{p}$ calculations and experiments we find a topological transition from the topological nontrivial quantum spin Hall state into a trivial insulator with decreasing QW thickness. The spatial localization near the interfaces and the spin polarization are demonstrated for the edge states for QWs with thicknesses near the critical one. They do not depend on the QW orientation and are therefore topologically protected. Below the critical QW thickness, the trivial insulator exhibits drastic confinement effects with a significant gap opening. We show that the inclusion of inversion symmetry, the nonaxial rotation symmetry of the QWs, and the real QW barriers lead to some agreement but also significant deviations from the predictions within toy models. The deviations concern the critical thickness, the number and localization of edge states, and the possibility to find QW subbands between edge states.

DOI: 10.1103/PhysRevB.89.195312 PACS number(s): 71.20.Nr, 71.70.Ej, 72.25.Mk

I. INTRODUCTION

The interplay between symmetry and topology can lead to very rich and profound physics of matter. In recent years, topological insulators (TIs) have attracted great attention as a topologically protected quantum state of matter originating from Bloch bands but with unique physical properties [1–5]. Three-dimensional (3D) TIs have a bulk band gap like an ordinary insulator but support conducting states on their edge or surface [6–8]. The U(1) and time-reversal symmetry together generate the nontrivial spectrum at a boundary. An odd number of relativistic Dirac fermions in the edge or surface states is characterized by their spin-polarized massless Dirac-cone-like (DC-like) dispersion. The unique properties of these electrons in states with a two-dimensional (2D) dispersion are considered to realize novel electronic and transport phenomena. The 2D TIs can be classified either into quantum Hall effect (QHE) or quantum spin Hall (QSH) effect states. The underlying physical origin, independent of dimensionality, of the topological property of TIs is the strong spin-orbit coupling (SOC), which may play a similar role as the Lorentz force in the QSH state.

The prototypical material for demonstration of properties of both 3D and 2D TIs is the zero-gap compound semiconductor HgTe which crystallizes in zinc-blende geometry with the space group T_d^2 ($F\bar{4}3m$). It possesses an inverted band structure. Because of strong relativistic mass-Darwin effects the Hg $6s$ states are below the Te $5p$ ones. Together with the strong SOC, an inverted band structure near the Γ point appears with the $s_{\frac{1}{2}}$-type band $\Gamma_{6c}^{(2)}$ below the $p_{\frac{3}{2}}$-type band $\Gamma_{8v}^{(4)}$ but still above the $p_{\frac{1}{2}}$-derived band $\Gamma_{7v}^{(2)}$ [9–11]. This band ordering is in agreement with photoemission data [12] and quasiparticle (QP) band-structure calculations within the GW approximation [13,14]. The large SOC-induced splitting of the $\Gamma_{8v}^{(4)}$ and $\Gamma_{7v}^{(2)}$ states is confirmed experimentally and theoretically as $\Delta_{SO} = 0.91$ eV [12,13] or a slightly smaller value $\Delta_{SO} = 0.80$ eV [14]. Without free carriers the Fermi level is pinned by the $\Gamma_{8v}^{(4)}$ states and, hence, separates the lowest empty conduction and highest occupied valence band by a zero gap at Γ. The resulting band structure is called to be an inverted one since the $\Gamma_{8v}^{(4)}$-$\Gamma_{6c}^{(2)}$ sp gap E_g is negative with values $E_g = -0.6$ to -0.3 eV [12–14].

The two-dimensional TI state was first predicted and observed in HgTe quantum wells (QWs) embedded between CdTe barrier layers [9,15]. Nonlocal transport measurements demonstrated edge-state transport without any contributions from carriers localized in the QWs. Using transport measurements, such spin currents can be observed [16]. When the thickness of the QWs is varied, the electronic structure seems to change from a normal to an inverted type to a critical thickness of about $d_c \approx 6.3$ nm [9,15]. This transition is claimed to be a topological transition between a conventional insulating phase (for small thicknesses $d < d_c$) and a phase corresponding to the QSH state with a single pair of helical edge states. The key feature of a QSH insulator is the presence of protected gapless edge states which carry two spin-polarized currents propagating in opposite directions [17]. However, there are open questions: (i) in real CdTe/HgTe/CdTe(001) quantum wells the QW thickness d can not be continuously varied as assumed by theory (and also experiment). For instance, the measured thickness $d_c = 6.3$ nm is not an integer multiple of the bulk lattice constant of about $a_0 = 0.6453$ nm [18]. (ii) Recent experiments on InAs/GaSb heterostuctures have shown similar results [19,20] despite the fact that both zinc-blende compounds do not possess an inverted band structure. (iii) The topological transition and the edge states should be independent of the growth direction of the QW structures. However, their realization has not been demonstrated within an atomic view on the interfaces. (iv) A clear proof of the spin polarization of the edge states is still missing. (v) In

*sebastian.kuefner@uni-jena.de

contrast to the applied theoretical toy models, the assumed inversion and axial rotation symmetry is reduced in real QWs.

HgTe is also expected to have DC-like surface bands [21,22], but because of its character as zero-gap semiconductor they should appear within the bulk bands. However, with applied biaxial or uniaxial strain parallel to the surface normal, the symmetry is lowered from cubic to tetragonal. The degeneracy of the $\Gamma_{8v}^{(4)}$ conduction and valence bands at Γ is lifted. A real gap is opened and the strained HgTe can serve as a real insulator in the bulk regions [23,24]. Dirac cones are expected to appear in this gap. This effect seems to be demonstrated by observation of quantized Hall effect that results from 2D single Dirac-cone-like topological surface states [25].

In this paper, we investigate the topological transition and the edge states in HgTe/CdTe multi-quantum-well structures by means of *ab initio* approaches to their atomic geometries and quasiparticle band structures including spin-orbit interaction. The thickness of the HgTe QWs is varied while the thickness of the CdTe barrier layers remains fixed. Two growth directions [001] and [110] and, hence, polar and nonpolar interfaces are investigated. The theoretical and computational methods are described in Sec. II. The results and discussions are presented in Sec. III. We study the resulting bulk electronic QP structures, the electrostatics in the heterosystems, and its consequences for the band discontinuities. This main section is concluded by the resulting 2D QP band structures and a description of edge states with Dirac cones and spin polarization. Finally, a summary and conclusions are given in Sec. IV.

II. THEORETICAL AND COMPUTATIONAL METHODS

For the total-energy calculations and structural optimizations, we apply the density functional theory (DFT) [26] within the local density approximation (LDA) [27] as implemented in the Vienna *ab initio* simulation package (VASP) [28,29]. Exchange and correlation are described using the results of Ceperly and Alder [30] as parametrized by Perdew and Zunger [31]. The electronic-structure calculations in the Kohn-Sham framework are performed including the scalar-relativistic effects and spin-orbit coupling [32]. The electron-ion interaction is described by pseudopotentials that are generated within the projector-augmented wave (PAW) method [33,34]. The Cd $4d$, Cd $5s$, Hg $5d$, Hg $6s$, Te $5s$, and Te $5p$ electrons are treated as valence electrons. While the single-particle wave functions in the core regions are also described by projector-augmented waves, they are expanded into a set of plane waves in the regions in-between the PAW spheres. A plane-wave basis set with an energy cutoff of 500 eV for bulk calculations or 275 eV for the superlattices is applied. Wave functions result in all-electron quality, i.e., with the correct node structure in the spheres. Bulk Brillouin zone (BZ) integrations are replaced by a sum over $12\times12\times12$ Monkhorst-Pack $\mathbf{k}$ points [35]. In the case of the superlattice calculations, the $\mathbf{k}$ space is sampled by a $6\times6\times1$ [$6\times4\times1$] Monkhorst-Pack mesh for the (001) [(110)] supercells. The optimized lattice constants of the zinc-blende materials $a_0 = 6.45$ Å (HgTe) and $a_0 = 6.46$ Å (CdTe) slightly deviate from the experimental values $a_0 = 6.453$ Å (HgTe) and $a_0 = 6.48$ Å (CdTe) [36], respectively, because of the used exchange-correlation (XC) potential and the neglect of zero-point vibrations. However, we have to point out, that in other data collections a measured value of $a_0 = 6.460$ Å [18] (CdTe), much closer to the theoretical lattice constant, has been published.

The Kohn-Sham eigenvalues computed by means of local or semilocal XC potentials significantly underestimate fundamental gaps and interband energy distances [37]. Moreover, in the case of zero-gap semiconductors, the wrong band ordering resulting in the negative ΓL gap and in an interchange of the $\Gamma_{6c}^{(2)}$ and $\Gamma_{7v}^{(2)}$ levels plays a role. This has been discussed in detail for α-Sn [38]. In the bulk case, the modeling of the XC self-energy by a spatially nonlocal XC potential applying an XC hybrid functional, for example, the HSE06 [39] one, already solves the majority of problems. However, such a method is computationally too expensive to be applied to systems with large unit cells as used for modeling of the multi-QW and superlattice stuctures. Therefore, we test and apply a poorman's method for the computation of quasiparticle band structures of superlattices that gives reasonable results for the bulk band structures but demands computational efforts comparable to that of DFT-LDA and, hence, is applicable to multi-QW structures. This is the Tran-Blaha method with the modified Becke-Johnson (MBJ) semilocal exchange functional [40], also called MBJLDA method. It corrects the error of a DFT-LDA band structure and can be easily combined with the inclusion of SOC. This has been demonstrated for many zinc-blende compounds [41,42]. Usually, the application of the MBJLDA is restricted to homogeneous systems without surfaces or interfaces because of a parameter CMBJ which is specific for one material. Fortunately, the parameter CMBJ $= 1.235$ is equal for HgTe and CdTe. This makes the application of this approximate quasiparticle theory possible for HgTe/CdTe superlattices (SLs).

A CdTe/HgTe/CdTe QW structure with a HgTe layer thickness d_1 is modeled by a corresponding multi-QW structure with a sufficient thickness d_2 of the CdTe barrier layers. Two growth directions [001] and [110] are studied. The CdTe wafers usually used as substrates are oriented along [001]. The (110) surface is the common cleavage face of all zinc-blende crystals. In practice, we investigate $(HgTe)_N(CdTe)_M(001)$ and $(HgTe)_N(CdTe)_M(110)$ superlattices with N HgTe double layers and the corresponding number of bilayers M in the CdTe case. We only study asymmetric heterostructures with even numbers N and M since an irreversible (001) [(110)] crystal slab contains four (two) atomic layers [43]. Since the (001) $\sqrt{2}\times\sqrt{2}$ [(110)1×1] surface unit cells are squares (rectangles), the superlattices with a lattice constant $(d_1 + d_2)$ defined by the $(N + M)$ bilayers possess a tetragonal (orthorhombic) symmetry. As examples, the unit cells of a $(HgTe)_{12}(CdTe)_4(110)$ superlattice and a $(HgTe)_{16}(CdTe)_4(001)$ superlattice are displayed in Fig. 1. In the unstrained limit, it would hold $d_1 = \frac{Na_{01}}{2}$ ($d_1 = \frac{Na_{01}}{\sqrt{2}}$) and $d_2 = \frac{Ma_{02}}{2}$ ($d_2 = \frac{Ma_{02}}{\sqrt{2}}$) for the [001] ([110]) orientation. In the (001) [(110)] case the two interfaces per SL unit cell Te-Hg and Te-Cd (CdTe-HgTe and HgTe-CdTe) are polar (nonpolar). Nonetheless, both the (001) and (001) double layers are electrically neutral. The number $M = 4$ of

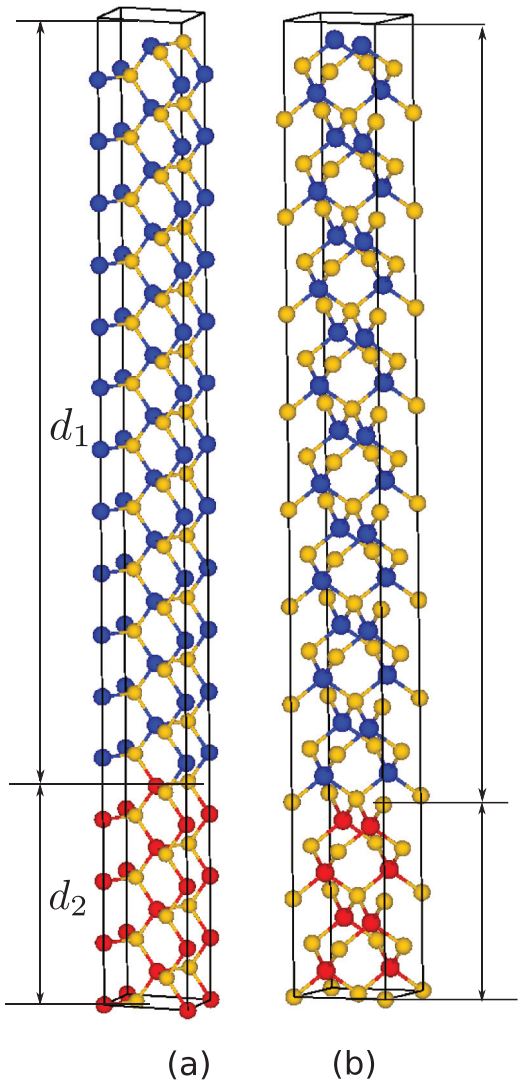

FIG. 1. (Color online) Unit cell of $(HgTe)_{12}(CdTe)_4(110)$ superlattice (a) and the $(HgTe)_{16}(CdTe)_4(001)$ superlattice (b). The Cd(Hg,Te) atoms are shown as red (blue, yellow) dots. In (b), a nonprimitive cell with a $\sqrt{2} \times \sqrt{2}$ lateral cell is displayed.

atomic bilayers of the barrier material is fixed both cases. It results in a CdTe thickness $d_2 = 1.6$ nm (1.13 nm) using the DFT-LDA lattice constant for (110) [(001)]. It is sufficiently thick to confine electrons and holes in the HgTe layers. We assume that only the HgTe layers are strained to adapt the lattice mismatch [44]. In agreement with experimental findings [17,25], we assume a 0.15 % tensile strain in the HgTe layers. In the explicit calculations we fix the in-plane lattice constants in accordance to the cubic lattice constant of CdTe, as derived by means of DFT-LDA. Then, using the ratio $R_b = -\frac{2C_{12}}{C_{11}} = -1.37$ [45] of the elastic constants and the misfit between the DFT-LDA lattice constants, the distances between bilayers (monolayers) in the [001] ([110]) direction are determined. The thickness of these layers varies between $d_1 = 0.9$–5.7 nm. The electronic-structure results are presented in a square- (rectangular-) shaped BZ for the (001) [(110)] systems.

III. RESULTS AND DISCUSSION

A. Bulk band structures

The QP band structures of the two zinc-blende compounds CdTe and HgTe are depicted in Fig. 2. Results of the two different approximate treatments are shown. The darkness of the dots characterizes the p character of the corresponding Bloch states. The barrier material CdTe [see Fig. 2(a)] has a normal band progression with the s-type $\Gamma_{6c}^{(2)}$ band lying above the p-type $\Gamma_{8v}^{(4)}$ and $\Gamma_{7v}^{(2)}$ bands. The positive gap $E_g = \varepsilon(\Gamma_{6c}) - \varepsilon(\Gamma_{8v})$ is opened from 0.298 eV (DFT-LDA) to 1.095 eV (HSE06) and 1.547 eV (MBJLDA). The latter value is in close agreement with room-temperature and low-temperature measured values 1.529 and 1.57 eV, respectively [46,47]. Therefore, it should be reasonable for studying the CdTe/HgTe band discontinuities and the confinement in CdTe/HgTe/CdTe QWs. The computed spin-orbit splittings between $\Gamma_{8v}^{(4)}$ and $\Gamma_{7v}^{(2)}$, $\Delta_{SO} = 0.78$ eV (LDA), 0.86 eV (HSE) and 0.71 eV (MBJLDA), are also in reasonable agreement with the measured value of $\Delta_{SO} = 0.95$ eV [18].

The band structures in Fig. 2 show that HgTe is, however, a zero-gap semiconductor with an inverted band ordering $\Gamma_{8v}^{(4)}$-$\Gamma_{6c}^{(2)}$-$\Gamma_{7v}^{(2)}$, compared to CdTe. The characteristic parameters $E_g = -1.12$ eV (LDA), -0.47 eV (HSE), and -0.26 eV (MBJLDA) are in reasonable agreement with the measured value $E_g = -0.29$ eV [12] if QP effects are taken into account. We have also studied the influence of compressive and tensile strain on the band structure of HgTe, in particular, the tetragonal splitting of the $\Gamma_{8v}^{(4)}$ levels and the ordering of these p-derived levels and the s-derived one $\Gamma_{6c}^{(2)}$. For biaxial strains smaller than 1%, the band ordering is conserved and the splitting of the $\Gamma_{8v}^{(4)}$ states is of the order of 10–20 meV. Only for unrealistic large strains of the order of 5% the band ordering is changed. Consequently, the influence of the small strain in the HgTe should be of minor influence compared to quantum size effects. Altogether, we claim that the MBJLDA approach is a reasonable method also to compute the QP electronic band structures of HgTe/CdTe heterostructures including possible topological states with a high accuracy with respect to the energetic positions.

B. Electrostatics and band offsets

The band structures in Fig. 2 indicate the formation of type-III heterostructures between the zero-gap semiconductor HgTe and a semiconductor with reasonable fundamental gap of more than 1 eV such as CdTe [48]. Although the bottom of the conduction subband and the top of the valence subband are formed in the same semiconductor layer, here HgTe, very similar to the type-I case with a finite positive gap [48], in the resulting type-III multi-quantum-well structure or superlattice the band should be almost continuously adjusted from a negative band gap to a zero one or even to a positive gap as a function of the HgTe thickness d_1. How this happens depends on the band discontinuities between HgTe and CdTe [49]. We discuss these quantities, in particular the (positive) valence band offset ΔE_v between the $\Gamma_{8v}^{(4)}$ level in HgTe and the $\Gamma_{8v}^{(4)}$ one in CdTe. The "conduction band" offset ΔE_c is more difficult to define because of the negative sp gap in HgTe. Nonetheless,

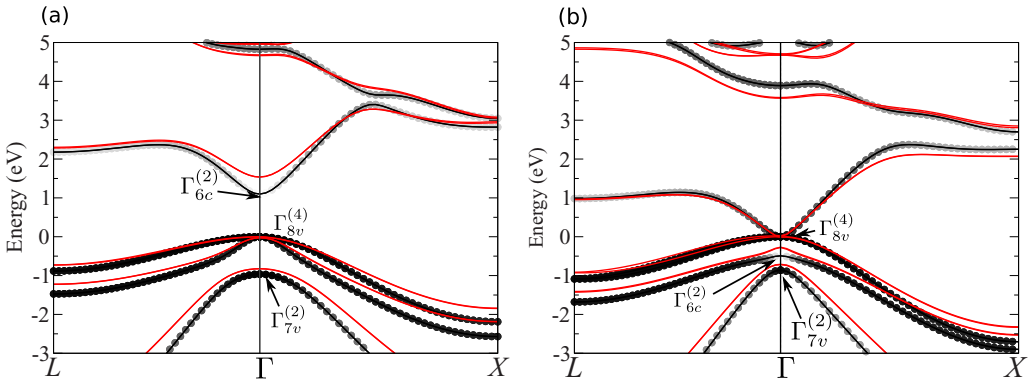

FIG. 2. (Color online) Band structures of CdTe (a) and HgTe (b) within the HSE06 hybrid functional (black solid lines) and MBJLDA (red solid lines) approach. The dots indicate the projection onto p orbitals. The darker a dot, the higher the p contribution. The $\Gamma_{8v}^{(4)}$ position is used as energy zero.

a reliable possibility could be the difference between the $\Gamma_{6c}^{(2)}$ levels in CdTe and HgTe.

The calculation of reasonable band offsets, which are comparable with experimental values, is difficult because of the presence of interfaces. The so-called natural band discontinuities can give a first approach by aligning the corresponding two bulk band structures. One reasonable possibility is the use of the branch points E_B [49–51]. The main idea is the existence of a charge neutrality level in the fundamental gap, where the character of electronic states changes from acceptorlike to donorlike. We use the approximate method of Schleife *et al.* [51], which leads to band discontinuities for cubic and hexagonal compounds in reasonable agreement with experimental data for many semiconductors [51,52]. With respect to the $\Gamma_{8v}^{(4)}$ position, we find $E_B = 0.71$ eV (CdTe) and 0.10 eV (HgTe) in great agreement with results of other computations [49]. The resulting natural band discontinuity $\Delta E_v = 0.72$ eV is still smaller than the fundamental gap of CdTe but too large in comparison with other calculations and measured values [47,49,53,54]. The resulting large values of ΔE_v indicate that the branch-point method might not be applicable to HgTe/CdTe heterosystems.

The determination of the band offsets by the alignment of branch points derived from bulk band-structure calculations neglects effects of the real interfaces and the electrostatics in heterostructures [52,55]. Another problem in real QW structures is related to confinement of electrons and holes in HgTe that should reduce the band discontinuities. Therefore, in a second approach, we determine the valence band discontinuities using the electrostatic potentials $V_{es}(z)$ derived from the local part of the Kohn-Sham one with z parallel to the SL axis of the investigated HgTe/CdTe superlattices and the corresponding bulk systems. As the energetic positions of the bulk band edges $\Gamma_{8v}^{(4)}$ and $\Gamma_{6c}^{(2)}$ relative to the bulk potentials $V_{es}(z)$ are known, the band discontinuities of a given superlattice can be formally derived from the comparison of $V_{es}(z)$ for bulk compounds and the superlattice. This procedure is visualized in Fig. 3 for the (110) case. The direct comparison is possible since the amplitudes and widths of the oscillations with the atomic layers remain the same in the superlattices, independent of the interfaces, their distances, and the small confinement in the HgTe layers. Only the relative position of the oscillations in the HgTe and CdTe layers seems to be influenced, mainly by the electrostatics in the superlattice.

The resulting valence band discontinuities ΔE_v between HgTe and CdTe are summarized in Table I. They depend on the HgTe QW thickness d_1 and the QW orientation [110] and [001]. As a surprise, the ΔE_v values decrease with increasing thickness d_1. The electronic confinement of the holes would lead to an opposite tendency. The effect visible in Table I is mainly due to the superlattice electrostatics, including different dipole-potential steps for the different HgTe layer thicknesses. For small QW thicknesses $d_1 < 3$ nm, the results are in excellent accordance with more recent experimental findings of $\Delta E_v = 0.53$ eV [47]. For intermediate thicknesses $d_1 \approx 4$ nm, the results in Table I are close to values $\Delta E_v = 0.35 \pm 0.06$ eV from earlier measurements [49]. The ΔE_v calculated for the largest QW thicknesses are small, in agreement with the early assumptions of vanishing valence band offsets based on the common-anion rule [21,43]. The

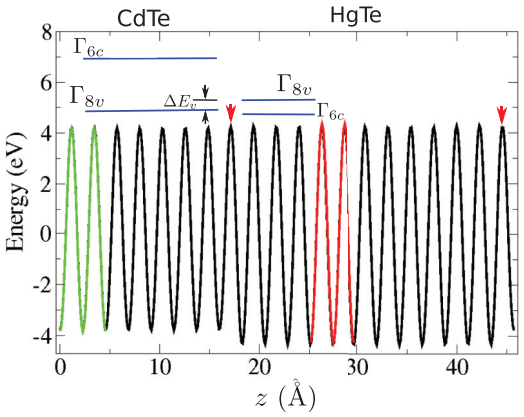

FIG. 3. (Color online) Plane-averaged electrostatic potential $V_{es}(z)$ (black line) of a $(HgTe)_6(CdTe)_4(110)$ superlattice with a period $d_1 + d_2 = 47$ Å. Two oscillations of the potentials of HgTe bulk (red line) and CdTe (green line), used for alignment of band states, are depicted. Since the relative positions of the bulk band edges are known (see blue levels in inset), the valence band discontinuity ΔE_v can be directly read. The space-averaged electrostatic potential of the superlattice is used as absolute energy zero. The vertical red arrows indicate the interface positions.

TABLE I. Resulting valence band discontinuities for (110) and (001) HgTe-CdTe QWs depending on the QW thickness d_1 or number of bilayers. The positive sign indicates that the HgTe Γ_8 level is inside the CdTe gap.

QW thickness		Orientation	
		ΔE_v	(eV)
d_1 (nm)	N	[110]	[001]
0.9	2	0.53	
2.1	6		0.45
2.8	6	0.48	
4.0	12		0.37
4.5	14		0.25
4.8	10	0.23	
5.3	16		0.18
5.7	12	0.13	

observed tendency is rather independent of the QW orientation. For relatively small QW thicknesses of $d_1 = 2.1$ nm ([001]) and 2.8 nm ([110]), the offsets only differ by 30 meV. However, it is questionable if the determination of band discontinuities does make sense for HgTe layers smaller than 1 nm as has been done in Ref. [47] because it is improbable that such a small layer behaves like HgTe bulk. In any case, the valence band offsets in Table I indicate that at least one hole state should be confined in the HgTe layers independent of the actual value d_1.

C. Electronic structure of $(HgTe)_N(CdTe)_4$(110) superlattices

The QP subband structures of the $(HgTe)_N(CdTe)_4$ (110) multi-QW structures with varying well thicknesses $N = 6$, 10, and 12 are displayed in Fig. 4. They are derived from those of the corresponding superlattices and plot versus the 2D BZ of the (110)1×1 interface [43] around the Γ point in the directions $\Gamma X \parallel [001]$ (toward the midpoint of an edge) and $\Gamma X' \parallel [1\bar{1}0]$ (toward the midpoint of the other edge) in a relatively small energy interval around the Fermi energy. The subbands are mainly derived from HgTe states. Only the lower occupied subbands possess contributions from CdTe as indicated by the energetic overlap with the projected bulk valence band structure of CdTe in Fig. 4. All heterostructures represent insulators with an extremely small fundamental gap at Γ for the SLs with $N = 10$ or 12. The bands along $\Gamma X'$ show a splitting mainly for the p-derived valence subbands, indicating the reduced point-group symmetry of the rectangular (110)1×1 unit cells compared to the (001) $\sqrt{2} \times \sqrt{2}$ unit cells from C_{2v} to D_{2d}. The $\mathbf{k}$-induced energy splitting of the subbands outside Γ along $\Gamma X'$ is mainly due to spin-orbit interaction. All these splittings are not visible in a $\mathbf{k} \cdot \mathbf{p}$ or tight-binding theory [9,23,56] because a higher symmetry, an axial rotation symmetry in the planes parallel to the interfaces, is accounted for. Only the empirical tight-binding theory with an interatomic SOC [24] accounts for such a splitting.

The subband structures in Fig. 4 exhibit a drastic variation with the thickness N or d_1 of the HgTe QWs due to confinement effects on electron and hole states and the band ordering related to relativistic effects. They modify the s and p character of the subband states, which is determined by a projection technique. In order to classify the (sub)band ordering, we study in detail their orbital character at Γ with varying QW thickness. The lowest-energy p- and hence $\Gamma_{8v}^{(4)}$-derived subband may contain holes (H) in conventional semiconductor band structures such as CdTe. The highest-energy s- and hence $\Gamma_{6c}^{(2)}$-derived subband may be an electron (E) band for normal band ordering. For $d_1 < 4.8$ nm in Fig. 4(a) the orbital-symmetry projections show that the two degenerate bands at Γ directly above the Fermi level are mainly formed by s orbitals, whereas in the subband below the Fermi level at Γ the projections onto p orbitals dominate. A trivial insulator with a similar ordering of the band symmetries as in bulk CdTe appears in the HgTe QWs. For large enough thicknesses d_1, e.g., $d_1 = 5.7$ nm, the subbands of the QW structure are inverted in agreement with the bulk band structure of HgTe in Fig. 2(a). The inverted subband structure, especially the inversion between E and H subbands near Γ, leads to the occurrence of the quantum spin Hall effect, i.e., a topologically nontrivial phase [15,16]. When the thickness of the QW is decreased, the energy of the H (E) subband increases (decreases) as a result of the quantum confinement. As a consequence, formally a level crossing should appear at $d_c \approx 4.6$ nm as described in Fig. 5. A further increase of the HgTe thickness toward $d_1 = 5.7$ nm as shown in Fig. 4(c) causes an inversion of the energetic ordering of s- and p-derived subbands toward the bulk situation of HgTe. In summary, a transition from a trivial insulator for $d < d_c$ to a topologically nontrivial QSH phase for $d > d_c$ is observed. We have to mention that the critical thickness d_c derived from Fig. 5 is somewhat smaller than the corresponding thicknesses derived theoretically from toy models [9,23]. The reasons are (i) that the true symmetry is broken down to the axial rotation symmetry around the interface normal and inversion symmetry, (ii) the consideration of only four bulk bands, and (iii) the neglect of interfaces and true energy barriers. The *ab initio* value of d_c is also smaller than the experimental value [15]. Experimentally, the QW thicknesses are taken from the growth data for modulation-doped HgTe/$Hg_{0.3}Cd_{0.7}$Te QW structures fabricated by molecular beam epitaxy [15]. The findings indicate that the nominal 5.5-nm structure shows the behavior of a trivial insulator, while the 7.3-nm structure exhibits the QSH insulator state. The thicknesses have been calibrated by x-ray reflectivity measurements. The reduced Cd content and, hence, the much smaller barriers make the precise classification of an interface position unlikely and may change the critical thickness d_c.

Most interesting is the intermediate region with an almost vanishing gap at Γ. For instance, for $d_1 = 4.8$ nm [Fig. 4(b)], the lowest empty and highest occupied subbands are nearly degenerate at Γ and show a linear $\mathbf{k}$ dispersion in all directions parallel to the interfaces with a Fermi velocity of $v_F = 0.69 \times 10^6$ m/s in the $\Gamma \rightarrow X$ direction. As a result Dirac cones, although slightly smoothed off near their apex due to the gap opening, are formed. However, the orbital picture is somewhat different from that which was predicted from toy models. The linear conical bands near Γ do not only consist of p states. Rather, s contributions are observed in the first empty subband, i.e., in the upper Dirac cone. Near the level crossing, some orbital mixing appears in contrast to the model studies [9,23]. Moreover, there are drastic differences between the empty and the occupied subbands. In the occupied case,

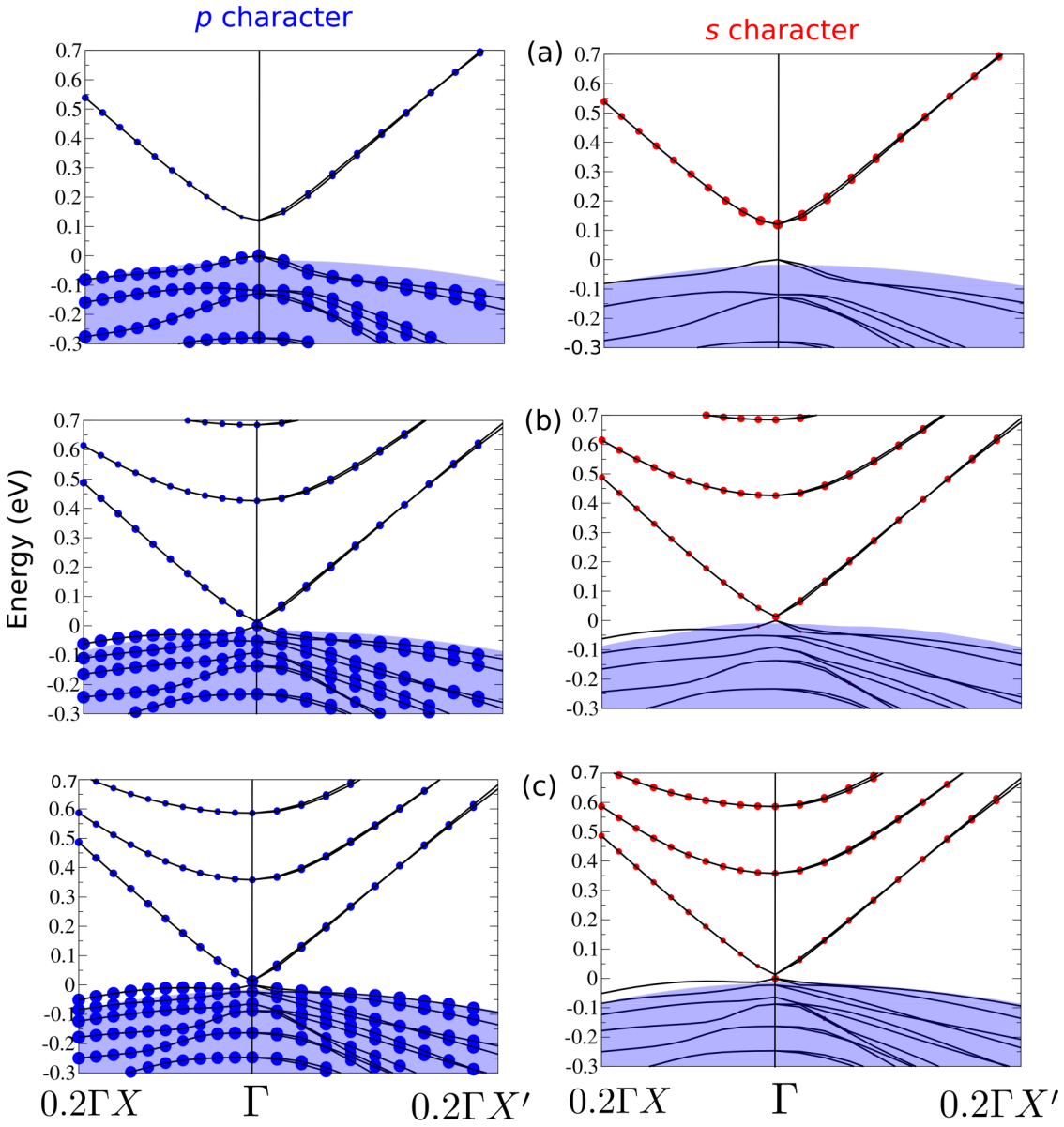

FIG. 4. (Color online) Subband structures of $(HgTe)_N(CdTe)_4(110)$ superlattices for varying QW thickness d_1: (a) 2.8 nm ($N = 6$), (b) 4.8 nm ($N = 10$), and (c) 5.7 nm ($N = 12$). The size of the dots visualizes the projection of the respective SL states onto atomic p orbitals (left panels) and atomic s orbitals (right panels). The larger the dots are, the higher the respective contributions. The blue background indicates the projected bulk band structure of CdTe. The energy of the highest occupied state of the SL is used as energy zero.

the linear character is restricted to an extremely small region around Γ. The four states forming the Dirac cones show strong atomlike p contributions. Of course, they are weaker for the lowest electron subbands because of the intermixing with s states. Apart from the apex regions, these cones mimic a direct QW realization of massless Dirac fermions, electrons, and holes. We can not confirm the predictions by means of a tight-binding method that the bulk inversion asymmetry of the zinc-blende structure leads to a shift from the center of the BZ to asymmetric **k** points near Γ where an actual crossing of the E and H bands happens, at least partially due to the SOC-induced band splitting discussed above [24]. One reason could be an overestimation of the interatomic SOC within the tight-binding method because it uses the same matrix element as for the intra-atomic SOC. We observe a striking difference for the HgTe QW with the thickness $d_2 = 5.7$ nm. The bands around the Fermi level are very similar with respect to the shape of the Dirac cones and the absolute energy values. However, the uppermost occupied states at Γ become a strong s character in contrast to the lowest empty subband. This effect can be interpreted as the beginning of the band inversion, at least at Γ.

In order to find out the relation of the Dirac-cone-like features to edge states, we plot in Fig. 6(a) the subband dispersion around Γ along $-X \rightarrow \Gamma \rightarrow X$ for the highest occupied and the lowest empty states together with their wave functions and their local spin orientations at Γ for the QW structure with $d = 4.8$ nm, i.e., the closest value to the critical thickness [for its band structure, see Fig. 4(b)]. The linear band dispersion, especially for the empty subband, is underlined,

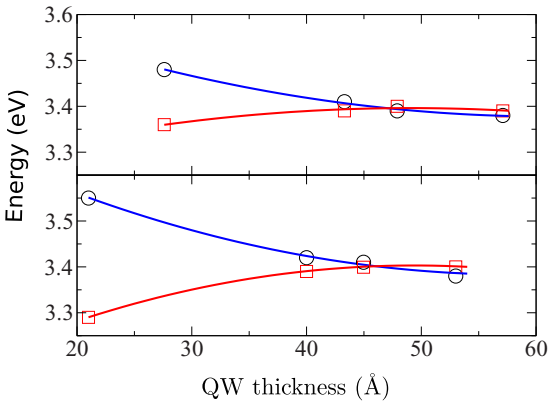

FIG. 5. (Color online) Thickness variation of s- and p-derived subband energies E (blue) and H (red) at Γ for the (110) (upper panel) and (001) (lower panel). The cubic interpolation of the band energies indicates a level crossing.

whereas this property is quickly modified away from Γ. From the Γ-point wave-function squares in Fig. 6(b) it is obvious that the highest occupied and lowest empty states are mainly located inside the HgTe layer. The atomic oscillations are clearly visible. Their envelopes, however, demonstrate the edge character. The maximum probability to find an electron is mainly localized at the HgTe-CdTe interfaces, i.e., at the edges of the QW, and decays exponentially into the HgTe layer, while the probability in the barrier layers is small, in particular for the hole state. The two edges belong to different spin orientations, which, however are influenced by the vector character of the spin [for demonstration, see Figs. 6(c)–6(e)] because of the used noncollinear treatment, and the different contributions of anions and cations. The helical character is also clearly visible. Moreover, the local magnetization [see Figs. 6(c)–6(e)] shows a rotation of π of the spin polarization between the $-X \rightarrow \Gamma$ and the $\Gamma \rightarrow X$ directions. This behavior is indicated by the colors of the bands in Fig. 6(a). The switch between $-X \rightarrow \Gamma$ with a certain spin orientation and $\Gamma \rightarrow X$ with another one is a consequence of the time-reversal symmetry. From Fig. 6(e) it is obvious that the lowest unoccupied state near Γ shows opposite spin orientations at the two edges. The resulting spin polarization together with the linear dispersion of the underlying band is a clear indication for the topological character of the state. The fact that they are topologically protected will be demonstrated below by its independence of the QW orientation. Here, we have used the term "edge state" in agreement with many previous papers on topological states in HgTe QW structures [9,16,24]. In comparison with 3D TIs with gapless topological states, this term has to be used with caution. "Edge" now refers to the interface between HgTe and CdTe and not to the surface of a certain insulator. Moreover, the energy barriers for electrons and holes at such interfaces are small (see Table I) in comparison to the surface barriers.

The dependence of the edge character of the highest occupied and lowest empty states on the QW thickness d_1 is visualized in Fig. 7. Their wave-function squares are plotted along the interface normals. The atomic oscillations are clearly visible. The variation of the maxima may be interpreted as the behavior of an envelope function, which may be comparable with results of the $\mathbf{k} \cdot \mathbf{p}$ theory. Near the topological transition,

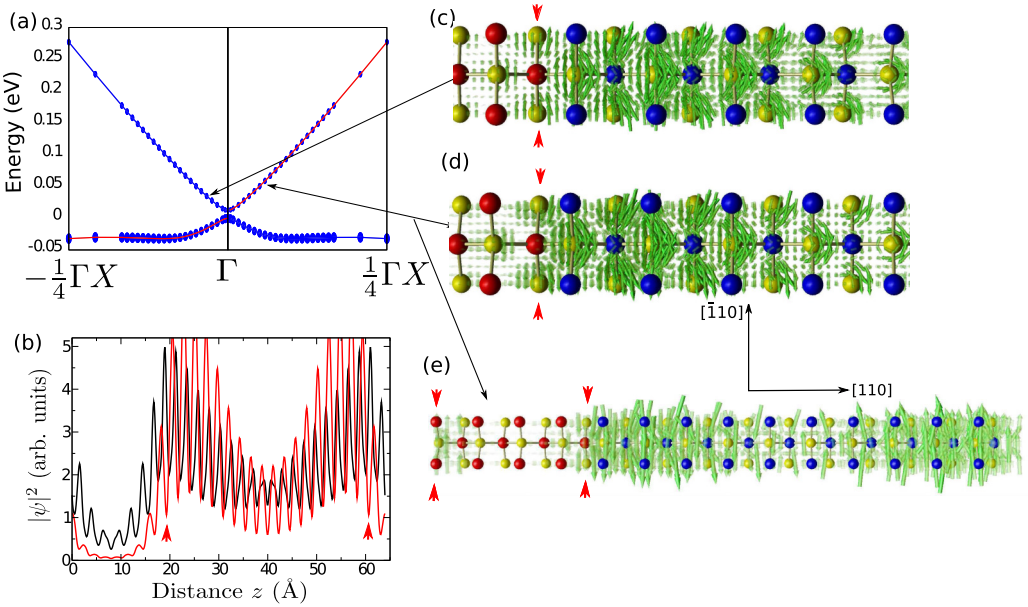

FIG. 6. (Color online) Characteristic edge-state properties in the case of the $N = 10$ (110) QW: (a) Dispersion of the highest occupied and lowest unoccupied subbands around Γ. The size of the blue dots indicates the atomic p contributions. The larger a dot, the higher the projection onto atomic p orbitals. The energy of the highest occupied state is used as energy zero. The colors of the bands, red or blue, indicate the direction of the local magnetization, the spin density, inside the rectangular surface BZ. (b) Wave-function square of the lowest unoccupied (black) and highest occupied states at Γ averaged over planes perpendicular to the QW orientation [110] as a function of the distance. A local magnetization with a large projection onto the [100] direction is depicted in red, while a blue color means a magnetization in the opposite direction. A view along a (001) plane of the local magnetization of the lowest unoccupied state in both cases is shown in (c) and (d). The spin polarization inside the whole supercell of the lowest unoccupied state near Γ is depicted in panel (e). Red arrows indicate the position of the interfaces.

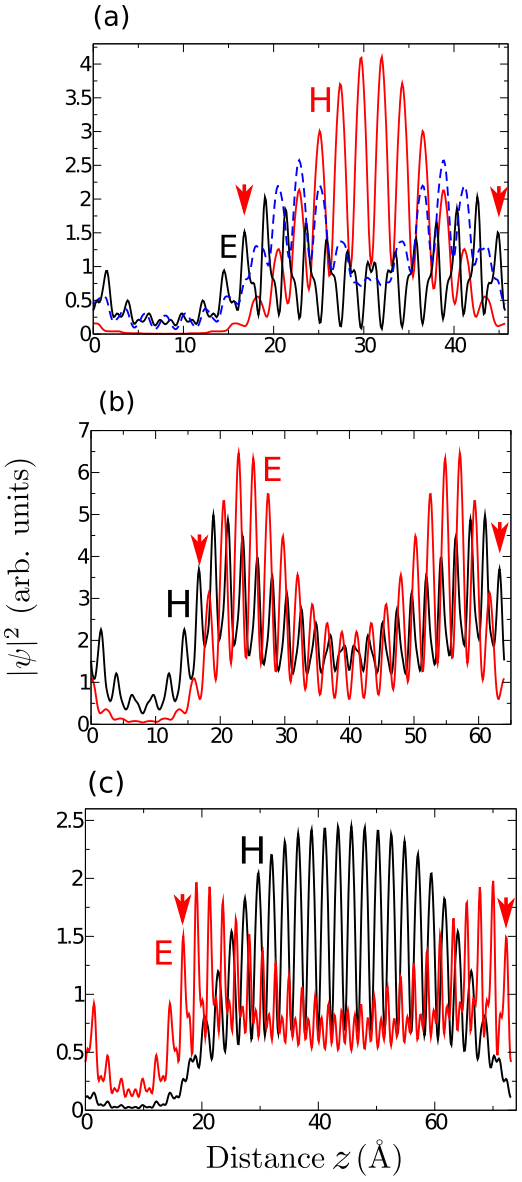

FIG. 7. (Color online) Wave-function square of the lowest unoccupied (black), the highest occupied (red), and the second-highest occupied (blue) states at Γ averaged over planes perpendicular to the QW orientation [110] as a function of the distance z for different QW thicknesses of 2.8 nm (a), 4.8 nm (b), and 5.7 nm (c). Red arrows indicate the position of the interfaces. Additionally, the E (H) character of the considered states is denoted inside the panels.

i.e., at $d_1 = 4.8$ nm, the states directly above and below the Fermi level both possess edge-state character as described above [see Figs. 6(a) and 7(b)]. However, from Fig. 7(a), it follows that the picture completely changes for $d_1 < 4.8$ nm. In contrast to the classification of the QW structure as a trivial insulator, the state directly above the Fermi level still shows edge character, whereas the envelope function of the state directly below the Fermi level shows clearly the shape of a typical $n = 1$ confined QW state with one maximum inside the HgTe layer. The character of the state below this QW state is difficult to interpret. It still shows partially the shape of an edge state. However, it may also be identified as an $n = 2$ state in a rectangular QW. In the case of $d_1 > 4.8$ nm, for example at $d_1 = 5.7$ nm, that has been classified as quantum-spin Hall phase, the highest occupied state exhibits edge-state character, whereas the lowest empty state is a QW state as shown in Fig. 7(c). It can be concluded that the inversion of the band symmetries at $d = d_c$ causes a significant change of the character of the states closest to the Fermi level. However, their edge character found in the transition region is not completely lost for thicknesses d_1 away from the critical one. QW states with strong p character keep some properties of an edge state independent of their occupation. The transport measurements [16] of n-modulation-doped HgTe/$Hg_{0.3}Cd_{0.7}$Te structures indicate transport in edge states despite a thickness above the critical one. According to Fig. 7(c) the electrons are, however, filled into an $n = 1$ QW state. Nonetheless, one has to take in mind that for the low-barrier material the situation could be closer to the situation depicted in Fig. 7(b) where indeed electrons are filled into the corresponding edge state which we should not only discuss in terms of its localization. In a small range around the Γ point, even the $n = 1$ QW state in Fig. 7(c) gives rise to a subband with linear dispersion. However, the low-barrier $Hg_{0.3}Cd_{0.7}$Te material may change the situation drastically with respect to the character of the lowest subband states at Γ but also with respect to the enlargement of the critical thickness d_c.

D. Electronic structure of $(HgTe)_N(CdTe)_4$(001) superlattices

The QP band structures of three superlattices with the thicknesses of $N = 6$, 12, and 16 bilayers of the HgTe(001) QWs are presented in Fig. 8 along two equivalent high-symmetry directions in the 2D quadratic BZ. They resemble qualitatively the behavior found in Fig. 4 for the (110) QWs. The smallest QWs exhibit QW states forming a significant fundamental sp gap and, hence, indicating a trivial insulator. The conduction subband edge is formed by s states, whereas p orbitals dominate the symmetry of the highest valence subband at Γ. For $d_1 = 2.1$ nm, the gap value amounts to 0.3 eV. In terms of confinement energies of rectangular quantum wells with a reduced mass of electron and hole of about one free-electron mass, this gap value is explainable together with the negative bulk gap.

The gap and the orbital character of band-edge states remarkably change with increasing thickness of d_1. For $d_1 = 4.5$ nm ($N = 14$), we find strong atomic p contributions to the wave function of the valence and conduction band edges This happens already for $d_1 = 4.0$ nm ($N = 12$) (not shown in Fig. 8). The fundamental gap between the occupied and empty states at Γ becomes very small with 10 meV, indicating the crossing of the levels, slightly modified by the tetragonal symmetry distortion. As a consequence, the corresponding bands with an approximate linear dispersion show slightly distorted Dirac cones near the Γ point. As in Fig. 4, linear bands are more pronounced for the lowest empty subband compared to the highest occupied one. Its Fermi velocity $v_F = 0.81$ m/s amounts to a similar value as in the (110) case. The behavior of the E and H subbands around the Fermi level versus the QW thickness is also displayed in Fig. 5. Similar to the (110) case, a critical thickness of about $d_c \approx 4.6$ nm is observed. Here, the atomistic nature of matter becomes evident. The thickness

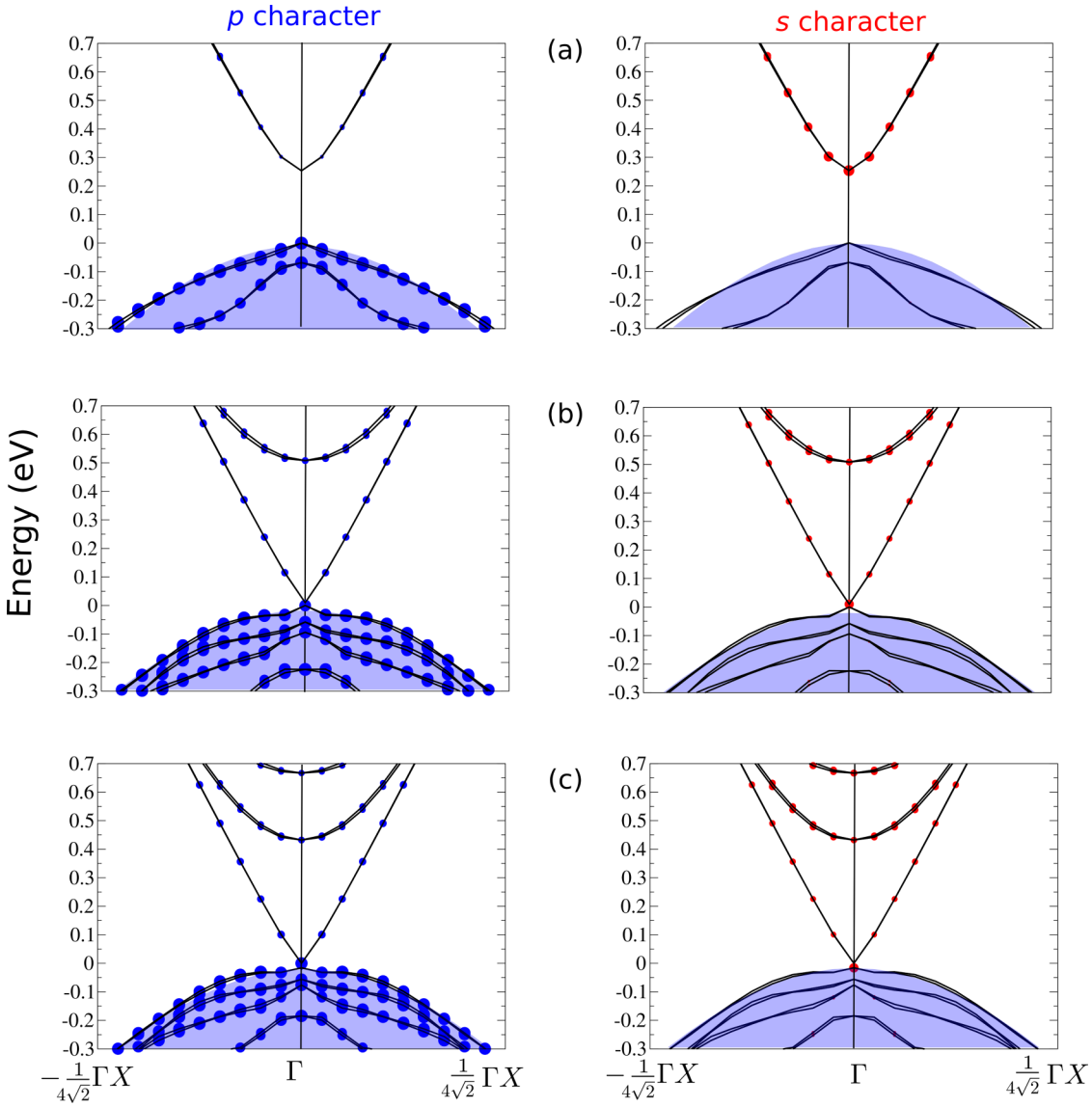

FIG. 8. (Color online) Subband structures of $(HgTe)_N(CdTe)_4(001)$ superlattices for varying QW thickness d_1: (a) 2.1 nm ($N = 6$), (b) 4.5 nm ($N = 14$), (c) 5.3 nm ($N = 16$). The dots visualize the projection of the respective SL states onto atomic p orbitals (left panels) and atomic s orbitals (right panels). The larger the dots, the higher the respective contributions. The energy of the highest occupied state is used as energy zero. The aligned projected bulk valence bands of CdTe are indicated by the blue regions.

can only be increased by double layers of HgTe as explained above and therefore there is no superlattice exactly at the transition point with the highest occupied as well as the lowest unoccupied state being an edge state in contrast to the $N = 10$ (110) QW that has been discussed in Sec. III C. For $d_1 > d_c$, again a nontrivial QSH insulator appears. However, the change in the subband structures from $d_1 = 4.5$ nm ($N = 14$) to $d_1 = 5.3$ nm ($N = 16$), i.e., the two QWs around the critical thickness, is rather negligible. The most striking effect is the interchange of the s and p character directly at Γ.

The dependence of the shape of the envelope functions of the states on the QW thickness d_1 that is depicted in Figs. 9(a)–9(c) is very similar to the case of (110) QWs as described in Sec. III C. Again, for $d_1 < d_c$, the highest occupied state is clearly a QW state, whereas the lowest empty state seemingly has edge-state character [see Fig. 9(a)]. In the case of $d_1 > d_c$ [see Fig. 9(c)], the situation is interchanged with respect to that of $d_1 < d_c$. For a thickness just above the critical one, the highest occupied state is an edge state, while the envelope of the lowest unoccupied state is described by an $n = 1$ QW state.

The formation of a QSH phase is accompanied by the occurrence of edge states. This is illustrated in Fig. 9(b) in the vicinity of the critical thickness $d_1 \approx d_c$, where states at Γ resemble edge states. The figure shows the wave-function squares of the lowest empty and highest occupied subband states at Γ of the $N = 12$ HgTe (001) QW. Their averages over xy planes perpendicular to the QW orientation exhibit the typical atomic oscillations along z, whereas their maxima also indicate their envelopes. The localization behavior of these states is similar to findings in Fig. 7(b) for a (110) QW. The envelope of the uppermost hole state indicates a localization in the HgTe layer with a behavior similar to $\sin^2(\frac{2\pi}{d_1^2})$ with $0 < z < d_1$, i.e., a maximum probability to find an electron

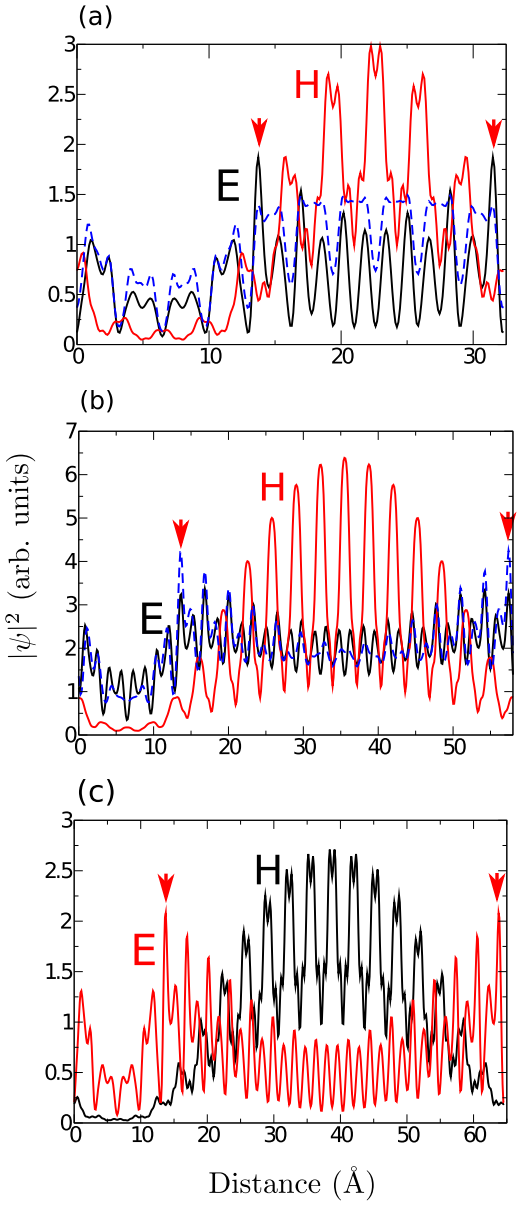

FIG. 9. (Color online) Wave-function square of the lowest unoccupied (black), the highest occupied (red), and the second-highest occupied (blue) states at Γ averaged over planes perpendicular to the QW orientation [001] as a function of the distance z for different QW thicknesses of 2.1 nm (a), 4.5 nm (b), and 5.3 nm (c). Red arrows indicate the positions of the interfaces. Additionally, the E (H) character of the considered states is denoted inside the panels.

in the center of the QW. This is clearly a QW state. By the way, the vanishing wave function in the CdTe layer indicates that the chosen barrier thickness $d_1 = 1.3$ nm is thick enough because of the relatively large band offsets. The first empty state is again an edge state as proven by its localization (shown) and its spin polarization (not shown). The second occupied state shows a rather identical spatial variation. The maximum probability to find an electron is localized in the HgTe QW near the interfaces but decays relative slowly into the QW center. Its spatial behavior is very similar to that of the edge state found for the HgTe (110) QWs in Fig. 7. It is to be independent of the QW orientation. This property to be protected, here not to be influenced by orientation, can be interpreted as a further verification of the topological nature of the studied state. Interestingly, the wave function of the second highest occupied state shows the same localization behavior as the electron state. This fact indicates that in a real quantum well structure around Γ the electronlike and holelike edge states may embed a conventional QW state. The main reason for those deviating findings from the (110) case is that the QW with $d_1 = 4.5$ nm is below critical thickness d_c, whereas the QW with $d_1 = 4.8$ nm that has been studied for the (110) orientation is slightly above d_c.

IV. SUMMARY AND CONCLUSIONS

We have applied an approximate quasiparticle method including spin-orbit interaction to study the size-dependent electronic properties of HgTe/CdTe multi-quantum-well structures. The method correctly describes the band distances, ordering, and splittings. It also leads to valence band discontinuities in agreement with experimental findings. However, we find that the electrostatics of the multi-QW systems depends on the layer thickness and therefore influences the alignment of the QP band structures of HgTe and CdTe in such heterosystems.

The resulting subband structures vary significantly with the QW thickness, although they are mainly derived by HgTe states, at least for energies close to and above the Fermi level. Despite the somewhat more complex electronic structures due to a symmetry lowering compared to a rotation axial symmetry and a fixed spin-orbit interaction, we qualitatively verify the predictions made by $\mathbf{k} \cdot \mathbf{p}$ theory and their experimental proof. A topological transition from a trivial insulator with normal band ordering for small thicknesses $d_1 < d_c$ to quantum spin Hall phase for $d_1 > d_c$ is confirmed. It approximately occurs for critical QW thicknesses $d_c \approx 4.6$ nm rather independent of the QW orientation. At the inversion transition thickness nearly linear bands appear at the Fermi level. They give rise to Dirac cones slightly modified due to a gap opening. This effect is most pronounced for the QW structures with a thickness only slightly above the critical one, as clearly demonstrated in the (110) case.

Most important for the demonstration of the QSH state are the observed edge states related to the lowest empty bands with almost linear dispersion. They show a similar behavior with respect to their localization and their spin distribution independent of the QW orientation. They are localized in the HgTe layers near the interfaces to CdTe but decay slowly into the QW. The clear spin polarization of these edge states indicates their possible contribution to spin currents near the edges, the interfaces. The picture of the quantum-phase transition and the edge states obtained from the quasiparticle calculations is much more complex than that derived from toy models with four bulk bands, no real barrier materials, and assumed axial rotation and inversion symmetry. Consequently, the following features have been found. (i) Two edge states only appear for QW thicknesses very close to the critical one. The corresponding states do generally not have 100% p-orbital symmetry. (ii) Dirac cones with linear bands are more pronounced for empty states. (iii) An edge state may

still occur for thicknesses smaller than the critical one, despite the normal band ordering and, hence, the identification of the HgTe/CdTe heterosystem as trivial insulator. Such an edge state also appears above d_c in the QSH state. However, its occupation is different from that in the trivial phase. For $d_1 > d_c$, the second edge state may be more separated, such that a normal QW state appears in-between. This fact has been demonstrated in the (001) case.

ACKNOWLEDGMENTS

We gratefully acknowledge financial support of the Austrian Fond zur Förderung der Wissenschaftlichen Forschung in the framework of SFB 25 Infrared Optical Nanostructures. The computations have been performed in part using the facilities of the John von Neumann Institute for Computing in Jülich.

[1] M. Z. Hasan and C. L. Kane, Rev. Mod. Phys. **82**, 3045 (2010).
[2] J. Moore, Nature (London) **464**, 194 (2010).
[3] X.-L. Qi and S.-C. Zhang, Rev. Mod. Phys. **83**, 1057 (2011).
[4] L. Müchler, H. Zhang, S. Chadov, Y. Binghai, F. Casper, J. Kübler, S. Zhang, and C. Felser, Angew. Chem. Int. Ed. **51**, 7221 (2012).
[5] Y. Ando, J. Phys. Soc. Jpn. **82**, 102001 (2013).
[6] J. E. Moore and L. Balents, Phys. Rev. B **75**, 121306 (2007).
[7] R. Roy, Phys. Rev. B **79**, 195322 (2009).
[8] L. Fu, C. L. Kane, and E. J. Mele, Phys. Rev. Lett. **98**, 106803 (2007).
[9] B. Andrei Bernevig, T. L. Hughes, and S.-C. Zhang, Science **314**, 1757 (2006).
[10] I. Tsidilkowski, *Gapless Semiconductors-a New Class of Materials* (Akademie-Verlag, Berlin, 1988).
[11] J. Vidal, X. Zhang, V. Stevanović, J.-W. Luo, and A. Zunger, Phys. Rev. B **86**, 075316 (2012).
[12] N. Orlowski, J. Augustin, Z. Gołacki, C. Janowitz, and R. Manzke, Phys. Rev. B **61**, R5058 (2000).
[13] R. Sakuma, C. Friedrich, T. Miyake, S. Blügel, and F. Aryasetiawan, Phys. Rev. B **84**, 085144 (2011).
[14] A. Svane, N. E. Christensen, M. Cardona, A. N. Chantis, M. van Schilfgaarde, and T. Kotani, Phys. Rev. B **84**, 205205 (2011).
[15] M. König, S. Wiedmann, C. Brüne, A. Roth, H. Buhmann, L. W. Molenkamp, X.-L. Qi, and S.-C. Zhang, Science **318**, 766 (2007).
[16] A. Roth, C. Brüne, H. Buhmann, L. W. Molenkamp, J. Maciejko, X.-L. Qi, and S.-C. Zhang, Science **325**, 294 (2009).
[17] K. C. Nowack, E. M. Spanton, M. Baenninger, M. König, J. R. Kirtley, B. Kalisky, C. Ames, P. Leubner, C. Brüne, H. Buhmann, L. W. Molenkamp, D. Goldhaber-Gordon, and Kathryn A. Moler, Nat. Mater. **12**, 787 (2013).
[18] W. Martienssen and H. Warlimont (eds.), *Springer Handbook of Condensed Matter and Materials Data* (Springer, Berlin, 2005).
[19] C. Liu, T. L. Hughes, X.-L. Qi, K. Wang, and S.-C. Zhang, Phys. Rev. Lett. **100**, 236601 (2008).
[20] I. Knez, R.-R. Du, and G. Sullivan, Phys. Rev. Lett. **107**, 136603 (2011).
[21] Y.-C. Chang, J. N. Schulman, G. Bastard, Y. Guldner, and M. Voos, Phys. Rev. B **31**, 2557 (1985).
[22] O. A. Pankratov, Semicond. Sci. Technol. **5**, S204 (1990).
[23] L. Fu and C. L. Kane, Phys. Rev. B **76**, 045302 (2007).
[24] X. Dai, T. L. Hughes, X.-L. Qi, Z. Fang, and S.-C. Zhang, Phys. Rev. B **77**, 125319 (2008).
[25] C. Brüne, C. X. Liu, E. G. Novik, E. M. Hankiewicz, H. Buhmann, Y. L. Chen, X. L. Qi, Z. X. Shen, S. C. Zhang, and L. W. Molenkamp, Phys. Rev. Lett. **106**, 126803 (2011).
[26] P. Hohenberg and W. Kohn, Phys. Rev. **136**, B864 (1964).
[27] W. Kohn and L. J. Sham, Phys. Rev. **140**, A1133 (1965).
[28] G. Kresse and J. Furthmüller, Phys. Rev. B **54**, 11169 (1996).
[29] G. Kresse and J. Furthmüller, Comp. Mater. Sci. **6**, 15 (1996).
[30] D. M. Ceperley and B. J. Alder, Phys. Rev. Lett. **45**, 566 (1980).
[31] J. P. Perdew and A. Zunger, Phys. Rev. B **23**, 5048 (1981).
[32] D. Hobbs, G. Kresse, and J. Hafner, Phys. Rev. B **62**, 11556 (2000).
[33] P. E. Blöchl, Phys. Rev. B **50**, 17953 (1994).
[34] G. Kresse and D. Joubert, Phys. Rev. B **59**, 1758 (1999).
[35] H. J. Monkhorst and J. D. Pack, Phys. Rev. B **13**, 5188 (1976).
[36] A. R. West, *Basic Solid State Chemistry* (Wiley, Chichester, UK, 1988).
[37] W. G. Aulbur, L. Jönsson, and J. W. Wilkins, in *Advances in Research and Applications*, Solid State Physics, Vol. 54, edited by H. Ehrenreich and F. Spaepen (Academic, New York, 1999), pp. 1–218.
[38] S. Küfner, J. Furthmüller, L. Matthes, M. Fitzner, and F. Bechstedt, Phys. Rev. B **87**, 235307 (2013).
[39] J. Heyd, G. E. Scuseria, and M. Ernzerhof, J. Chem. Phys. **118**, 8207 (2003).
[40] F. Tran and P. Blaha, Phys. Rev. Lett. **102**, 226401 (2009).
[41] Y.-S. Kim, M. Marsman, G. Kresse, F. Tran, and P. Blaha, Phys. Rev. B **82**, 205212 (2010).
[42] Y.-S. Kim, K. Hummer, and G. Kresse, Phys. Rev. B **80**, 035203 (2009).
[43] F. Bechstedt, *Principles of Surface Physics* (Springer, Berlin, 2003).
[44] J. N. Schulman and Y.-C. Chang, Phys. Rev. B **33**, 2594 (1986).
[45] J. Mavroides and D. Kolesar, Solid State Commun. **2**, 363 (1964).
[46] J. Camassel, D. Auvergne, H. Mathieu, R. Triboulet, and Y. Marfaing, Solid State Commun. **13**, 63 (1973).
[47] D. Eich, K. Ortner, U. Groh, Z. H. Chen, C. R. Becker, G. Landwehr, R. Fink, and E. Umbach, Physics Status Solidi A **173**, 261 (1999).
[48] P. Yu and M. Cardona, *Fundamentals of Semiconductors* (Springer, Berlin, 1996).
[49] H. Lüth, *Solid Surfaces, Interfaces and Thin Films* (Springer, Berlin, 2001).
[50] J. Tersoff, Phys. Rev. B **30**, 4874 (1984).
[51] A. Schleife, F. Fuchs, C. Rdl, J. Furthmller, and F. Bechstedt, Appl. Phys. Lett. **94**, 012104 (2009).

[52] B. Höffling, A. Schleife, C. Rödl, and F. Bechstedt, Phys. Rev. B **85**, 035305 (2012).
[53] A. Muoz, J. Sánchez-Dehesa, and F. Flores, Phys. Rev. B **37**, 4803 (1988).
[54] C. G. Van de Walle and R. M. Martin, Phys. Rev. B **37**, 4801 (1988).
[55] B. Höffling, A. Schleife, F. Fuchs, C. Rödl, and F. Bechstedt, Appl. Phys. Lett. **97**, 032116 (2010).
[56] B. Buttner, C. X. Liu, E. G. Tkachov, G.and Novik, C. Brune, H. Buhmann, E. M. Hankiewicz, P. Recher, B. Trauzettel, S. C. Zhang, and L. W. Molenkamp, Nat. Phys. **7**, 418 (2011).